Journal of Structural Geology 33 (2011) 1169–1177

Contents lists available at ScienceDirect

Journal of Structural Geology

journal homepage: www.elsevier.com/locate/jsg

# A rigid circular inclusion in an anisotropic host subject to simple shear

Marcin Dabrowski*, Daniel W. Schmid

*Physics of Geological Processes, University of Oslo, Oslo, Norway*

ARTICLE INFO

*Article history:*
Received 1 November 2010
Received in revised form
25 March 2011
Accepted 8 May 2011
Available online 23 May 2011

*Keywords:*
Porphyroblast
Inclusion
Anisotropy
Layers
Folding
Analytical

ABSTRACT

The solution for velocity and rate of deformation in an incompressible, homogeneously anisotropic viscous host embedding a cylindrical rigid inclusion subjected to a far-field shearing parallel to the anisotropy direction is presented. The rotation rate of the inclusion is equal to half the ambient shear rate independently of the anisotropy factor. The flow in the matrix localizes into conjugate shear bands sub-parallel to the anisotropy directions as the anisotropy factor increases. The presented anisotropic analytical solution, which neglects the bending stiffness, approximates the flow in a layered medium in the limit of infinitely thin layers. An initially planar layering is deflected adjacent to the inclusion and fold trains propagate into the host with progressing deformation. Numerical simulations show that the structural development leads to a decrease in the inclusion rotation rate and eventually to inclusion stagnation at high strains. The fold shapes become more angular and the fold trains reach further out into the host as the anisotropy factor is increased. Increasing the layering thickness (up to only 9 layers intercepting the inclusion) has no significant effect on how the layer inclusion rotation rate evolves with strain. A coarse layering in the host leads to a strongly reduced outreach of the fold trains and the absence of tight folds. The analytical solution, which is derived for a planar anisotropy in the host, can be employed to approximate the structural development for a weakly anisotropic host or small deformation. Structural development of an anisotropic medium plays a major role in determining the system behavior for large deformation.



## 1. Introduction

The reconstruction of tectonometamorphic processes is a matter of scrutinizing every scintilla of evidence. Nowadays, fine structures preserved internally within porphyroblasts can be accurately characterized using the Computed Tomography (CT) imaging technology (e.g., Huddlestone-Holmes and Ketcham, 2010). Despite their minute size, porphyroblast inclusion trails exhibit great potential of recording critical information regarding shear strain (Schoneveld, 1977), shear rate (Biermeier and Stuwe, 2003; Christensen et al., 1989), and style of folding (Jiang, 2001; Mancktelow and Visser, 1993; Williams and Jiang, 1999), to name a few.

Early models established the concurrent growth and rotation of porphyroblasts in a non-coaxial flow as the formation mechanism of snowball garnets that are characterized by spiral patterns of inclusion trails (Rosenfeld, 1970; Spry, 1963). Sigmoidal inclusion trails have been found less unambiguously indicative of the relative rotation of the porphyroblasts and the foliation, since they may develop due to post-tectonic helicitic growth over a crenulated foliation (Williams and Schoneveld, 1981). The inclusion patterns were investigated in numerical simulations, which adopted a linear viscous flow model and passive layers in the host, for different degrees of coupling at the inclusion–host interface (Bjornerud and Zhang, 1994) and in three-dimensions (Gray and Busa, 1994). The three-dimensional patterns obtained within the rotation model were found consistent with measured microstructures of snowball garnets (Williams and Jiang, 1999).

Nevertheless, the rotational behavior of porphyroblasts has been a subject of numerous studies that laid out an apparent conflict between mechanical models and geological observations. In a series of papers, the ability of garnets to rotate with respect to geographic coordinates was disputed by Bell et al. (Bell et al., 1992a,b; Bell and Johnson, 1989; Johnson, 1993). The modeling approach based on continuum mechanics was criticized as apparently incapable of representing anything else than a perfectly homogeneous isotropic medium and therefore inapplicable to rocks (Aerden, 2005) and Bell et al. (1993) blamed mathematics for being inadequate to handle highly heterogeneous systems.

Studying the rotation of porphyroblasts with respect to geographic coordinates was shown to be a misguided concept

* Corresponding author. Tel.: +47 41720506.
*E-mail address:* marcind@fys.uio.no (M. Dabrowski).

0191-8141/$ – see front matter © 2011 Elsevier Ltd. All rights reserved.
doi:10.1016/j.jsg.2011.05.003

(Jiang and Williams, 2004; Lister, 1993; Williams and Jiang, 1999). The conflict is altogether apparent, as noted by e.g., Bons et al. (2009), as both (i) a significant rotation of porphyroblast has been documented, and (ii) mechanical models can predict the stabilization, i.e. a vanishing rate of rotation with respect to principal flow directions, of rigid equidimensional inclusions under certain circumstances. The stabilization mechanisms for a circular rigid inclusion include the presence of a recrystallized weak rim (Schmid and Podladchikov, 2004), an incoherent porphyroblast–matrix interface (Bjornerud and Zhang, 1994), and shear localization (Johnson, 2009; ten Grotenhuis et al., 2002). The proposed models abandon the simple model of a homogeneous isotropic viscous embedding medium and a coherent grain–host interface, but still rely on the continuum mechanics approach.

In the heat of the debate, the fact that rocks hosting porphyroblasts are often strongly sheared and therefore likely to be anisotropic has been largely ignored. Only a few studies address the problem of mutual interaction of an inclusion and its anisotropic host. Fletcher (2009) showed that the rotation rate of an elliptical rigid inclusion embedded in a homogeneous anisotropic matrix is identical to the isotropic case. The question arises as to what extent the initial rotation rate persists in large deformation that results in deflection and folding of layers around the inclusion leading to a heterogeneous anisotropy. In their review paper juxtaposing conflicting opinions related to the rotational behavior of porphyroblasts, Passchier et al. (1992) wrote "As matters stand, we do not claim that we understand the complete behaviour of porphyroblasts in anisotropic media, …". After two decades, this fundamental issue still remains without an answer, even though the debate keeps rolling.

We investigate the rotation and structural evolution around a rigid circular inclusion embedded in a layered host that undergoes far-field layer-parallel simple shear. The effect of changing layer thickness on the rotation rate and structural development is investigated. In the limit of infinitely thin layers, an analytical solution is given for the initial state of a planar layering. A finite element model (FEM) is employed to study the effect of a discrete layering in the host. The FEM model is used to study a non-planar layering or anisotropy in large deformation. The potential of the analytical solution to approximate the finite strain evolution is investigated.

## 2. Model

### 2.1. Model setup

We study the flow around a circular rigid inclusion embedded in an anisotropic linear viscous matrix, see Fig. 1. The flow is assumed to be incompressible. In a complementary model, the matrix consists of discrete isotropic alternating layers. The viscosity ratio is set to ensure the same bulk anisotropic viscosity as in the primary model. The inclusion/matrix interface is welded and the inclusion radius is constant during deformation. The anisotropy is initially homogeneous or equivalently the lamination is planar. We focus on a layer-parallel simple shear. The symmetry of the model inhibits the translation of the inclusion and the inclusion motion is limited to the rotation.

### 2.2. Anisotropic model

The matrix anisotropy is described by two principal viscosities, $\mu_s$ in lamination-parallel shear, and $\mu_n$ in lamination-parallel shortening or extension. With coordinate axes and the principal axes of the anisotropy coinciding, the constitutive relations are

$$\begin{aligned} \sigma_{xx} &= -p + 2\mu_n D_{xx} \\ \sigma_{yy} &= -p + 2\mu_n D_{yy} \\ \sigma_{xy} &= 2\mu_s D_{xy} \end{aligned} \tag{1}$$

where $p$ denotes pressure, or negative of the mean stress, $\sigma_{xx}$, $\sigma_{yy}$, $\sigma_{xy}$ are the components of the stress tensor, and $D_{xx}$, $D_{yy}$, $D_{xy}$ are the components of the rate of deformation tensor. A two-dimensional incompressible plane flow is considered

$$D_{xx} + D_{yy} = 0, \quad D_{zz} = 0 \tag{2}$$

The degree of anisotropy is described by an anisotropy factor $\delta$

$$\delta = \frac{\mu_n}{\mu_s} \tag{3}$$

Stress equilibrium, with no body forces, under a creeping flow regime (Stokes flow) requires

$$\begin{aligned} \frac{\partial \sigma_{xx}}{\partial x} + \frac{\partial \sigma_{xy}}{\partial y} &= 0 \\ \frac{\partial \sigma_{xy}}{\partial x} + \frac{\partial \sigma_{yy}}{\partial y} &= 0 \end{aligned} \tag{4}$$

The constitutive relations (1) refer to the principal axes. When their orientation in the matrix is non-uniform, with finite deformation, a further development implemented in the numerical code is necessary. The constitutive relations must now be expressed so that they hold for principal axes arbitrarily orientated with respect to the fixed external reference axes $x$ and $y$. An evolution equation for this orientation that is concordant with the finite strain evolution of a layered medium is also required.

It is practical to introduce a vector field of unit vectors that are locally normal to the lamination $\vec{n}(\vec{x}, t)$. As the normal vectors remain in the $xy$-plane due to the plane flow condition, it suffices to describe their orientation using an angle $\varphi$ that measures the rotation between the normal vector and the axis $x$, i.e., $n_x = \cos\varphi$, $n_y = \sin\varphi$. The application of tensor transformation rules to (1) yields:

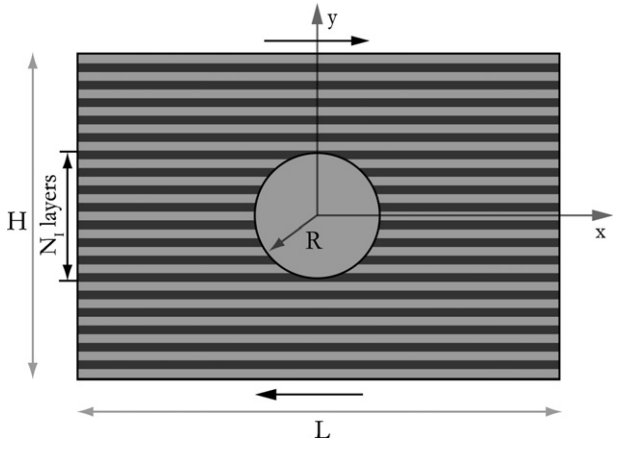


**Fig. 1.** A schematic representation of the studied model. A rigid circular inclusion of radius $R$ is placed in the center of a rectangular domain of a height $H$ and a width $L$. Equally spaced isotropic layers of high $\mu_1$ and low $\mu_2$ viscosity are present in the host and the layering is parallel to the shear direction. The number of individual layers intercepting the inclusion $N_l$ is varied. In the limit $N_l \to \infty$, the host is modeled as an anisotropic fluid with normal $\mu_n$ and shear $\mu_s$ viscosity with their ratio dictated by the viscosity ratio $\mu_2/\mu_1$. Constant horizontal velocity on the top and bottom walls is prescribed and periodic velocity is imposed on the lateral boundaries in numerical simulations. An analytical solution is presented for $R \ll H$ and $R \ll L$.

$$\begin{bmatrix}\sigma_{xx}+p\\ \sigma_{xy}\end{bmatrix}=\begin{bmatrix}\mu_n\cos^2 2\varphi+\mu_s\sin^2 2\varphi & (\mu_n-\mu_s)\sin 2\varphi\cos 2\varphi\\ (\mu_n-\mu_s)\sin 2\varphi\cos 2\varphi & \mu_n\sin^2 2\varphi+\mu_s\cos^2 2\varphi\end{bmatrix}\begin{bmatrix}D_{xx}\\ D_{xy}\end{bmatrix} \tag{5}$$

For a layered material, the evolution law for $\vec{n}$ is given by (e.g., Muhlhaus et al., 2002)

$$\frac{Dn_k}{Dt}=\left[W_{kp}-\left(D_{mk}n_m n_p-D_{pl}n_l n_k\right)\right]n_p \tag{6}$$

where $W$ denotes the vorticity tensor.

### 2.3. Effective anisotropy factor of a layered medium

The bulk response of a discretely layered medium at a scale of flow >> layer thickness may be approximated by an anisotropic continuum with a vanishing bending stiffness. The conditions under which this approximation is valid will be investigated. If the alternating layers have isotropic viscosities $\mu_1$ and $\mu_2$, and are present in thickness fractions $f_1$ and $f_2$, then (Biot, 1965):

$$\mu_n=f_1\mu_1+f_2\mu_2,\quad \mu_s=\left(\frac{f_1}{\mu_1}+\frac{f_2}{\mu_2}\right)^{-1} \tag{7}$$

The viscosities $\mu_s$ and $\mu_n$ are equal to the theoretical lower and upper bounds on the effective viscosity of the composite viscous medium for any configuration of the two isotropic components (Hill, 1952). Therefore, the anisotropy factor as defined by (2) exceeds unity for (6), i.e. the viscous resistance is higher in layer-parallel shortening/extension than in layer-parallel shearing. In this study we use equal thickness fractions $f_1=f_2=0.5$, for which

$$\delta=\frac{1}{4}\left(\sqrt{m}+\frac{1}{\sqrt{m}}\right)^2 \tag{8}$$

where the viscosity ratio $m=\mu_2/\mu_1$. At equal thickness fractions, the material has a maximum $\delta$ for a given $m$. Solving (7) with respect to $m$ results in

$$m=\frac{\sqrt{\delta}+\sqrt{\delta-1}}{\sqrt{\delta}-\sqrt{\delta-1}} \tag{9}$$

### 2.4. The initial state of planar lamination

Insight into the effect of matrix anisotropy is firstly provided by the study of the initial state of homogeneous planar lamination. An analytical solution for an elliptical inclusion in a homogeneous anisotropic matrix was derived by Willis (1964). The solution is given for an elastic medium, but it can easily be reduced to an incompressible viscous medium. Here, we consider the special case of a rigid circular inclusion of radius $R$ subjected to a far-field simple shear, with shear rate $\dot{\Gamma}^{\infty}=2D^{\infty}_{xy}$, parallel to the principal axis of anisotropy.

The velocity field that perturbs the background velocity field in the matrix is given by the following formula

$$V=i\frac{RD^{\infty}_{xy}}{4\gamma^2}\left[\gamma\left(\sqrt{X^+-4\gamma}-X^+-\sqrt{X^-+4\gamma}+X^-\right)+\left(\sqrt{\overline{X}^+-4\gamma}-\overline{X}^+-\sqrt{\overline{X}^-+4\gamma}+\overline{X}^-\right)\right] \tag{10}$$

where $X=x+iy$, $V=v_x+iv_y$, $i=\sqrt{1}$, $\gamma^2=(\sqrt{\delta}-1)/(\sqrt{\delta}+1)$, and the bar denotes the complex conjugate. The following coordinate transformation

$$X^{\pm}=X\pm\gamma\overline{X} \tag{11}$$

is used in (10). The net velocity field is obtained by adding the velocity field of the basic-state flow of simple shear to the perturbing velocity (10).

The magnitude of the perturbing velocity vector and half the shear rate (square root of the 2nd invariant of the rate of deformation tensor based on the net velocity field) are shown in Fig. 2. The weak anisotropy case, $\delta=2$, exhibits smooth variations approximating the isotropic case (cf. Schmid and Podladchikov, 2003). Increasing the anisotropy factor $\delta$ has a marked effect on the perturbation flow and here we analyze $\delta=100$ case, see Fig. 2f. The zones of high shear rate adjacent to the inclusion are enhanced and they merge to form shear bands (I) enclosing a square domain of low shear rate around the inclusion (II). The secondary maximum of shear rate (III), separated from the inclusion at small $\delta$, increases in magnitude and is located near the corners of the bounding square. Sharp conjugate shear bands (IV) extend in directions ~ parallel to the principal axes. The regions of low shear rate ($V$) of a width that equals the inclusion diameter follow the coordinate axes.

The rotation rate of the inclusion equals the far-field vorticity or half the rate of simple shear. The value can be explained using a symmetry argument (see Discussion) and is a particular example of a general result stating that the rotation rate of an elliptical rigid inclusion is not affected by a homogeneous anisotropy of the matrix (Fletcher, 2009).

### 2.5. Large deformation

Deformation around the inclusion changes the local orientation of the principal axes of the anisotropy in the matrix. However, it might be thought possible to obtain results using the analytical solution for a planar lamination to approximate the flow in the non-planar, non-uniform case. The displacement field obtained upon integrating the analytically obtained velocity field is used to move passive lines that are shown in the first column of Fig. 3. Here, we set the anisotropy factor at $\delta=10$ and study the system evolution up to shear strain $\Gamma^{\infty}=4$. As shown below, the structures obtained using the analytical solution provide a reasonable approximation to the true structural evolution up to shear strain of $\Gamma^{\infty}=1$ only.

The results of numerical experiments are presented in the remaining columns (see Appendix for details regarding the numerical implementation). The aspect ratio of the computational box was set at $L/H=2$, and the ratio between the inclusion radius and the box height $R/H=0.05$. Firstly, we discuss the $N_I=\infty$ case, i.e. the matrix is modeled as an anisotropic medium ($\delta=10$) and the orientation of the anisotropy is updated according to the local velocity gradient using (5) as the deformation progresses.

At $\Gamma^{\infty}=1$, the initial orthogonal symmetry of the rate of deformation field present is broken. Deformation is localized into a distinct band inclined at a high angle to the shear direction. This band coincides with the axis of the most prominent structure visible in the host formed by the gentle flexure of the markers. The zones of elevated shear rate adjacent to the inclusion are weakened.

At $\Gamma^{\infty}=1.6$, a secondary band of localized shearing has developed and links the inclusion and the primary high shear rate band. The secondary band is contained within a well-developed kink band that together with deflections related to the primary band encloses a structure similar to a box fold.

At $\Gamma^{\infty}=2$, the high shear rate bands merge into a more diffuse zone that is limited in outreach and inclined at 45° to the shear direction with a tendency to steepen towards the tips. Two subsidiary high shear rate bands have propagated vertically and

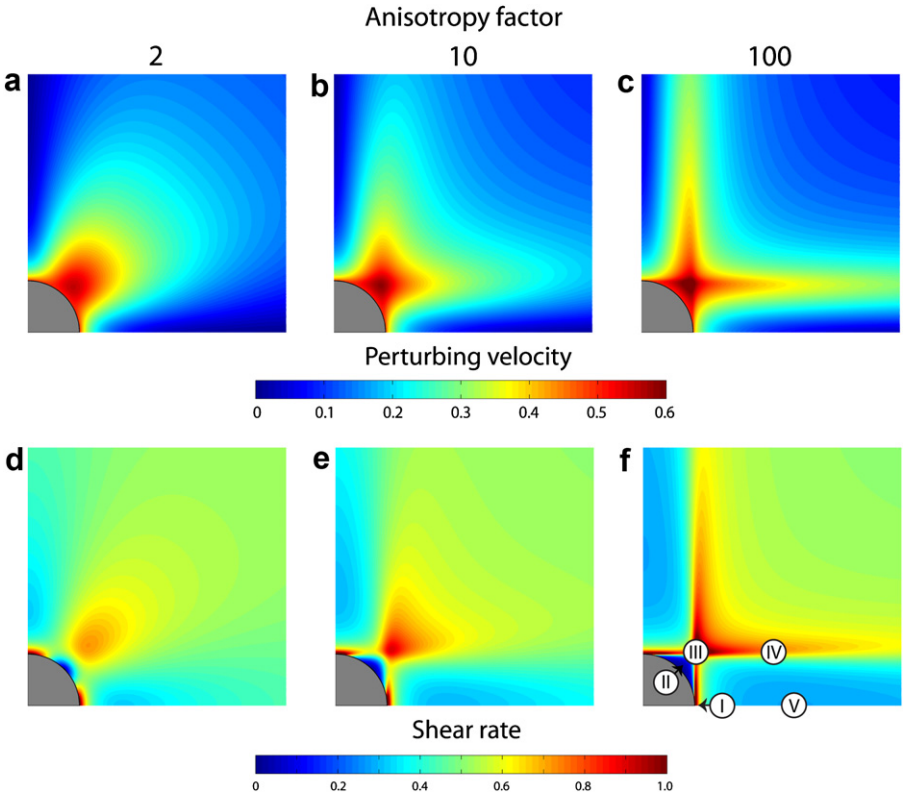


**Fig. 2.** The magnitude of velocity perturbation (a, b and c) and shear rate (d, e and f) around a rigid circular inclusion embedded in an infinite homogenous anisotropic host under far-field simple shear with the rate of a unit. Columns show analytically obtained results for the anisotropy factor $\delta = 2$, 10 and 100, respectively. Both fields are characterized by an orthotropic symmetry and the results are shown in a selected quadrant only.

horizontally from the main band near the inclusion, but these zones are diffuse and the flow is localized to a lesser degree. The horizontal band of low shear rate is now strongly enhanced. The structure is dominated by the kink band that has propagated and broadened partly in expense of the box fold interior.

At $\Gamma^{\infty} = 4$, the development of numerous diffuse bands of enhanced shear rate predominates. The primary kink band has been sheared and reoriented towards the shear plane and is now associated with a low shear rate. However, the kink band has not actively propagated further into the matrix. A secondary kink band of smaller range and amplitude has developed behind the primary kink band.

The results obtained for the discretely layered host ($N_l = 33$) are shown in the last column of Fig. 3. Here, the viscosity ratio of the isotropic layers is set correspondingly at $m \approx 38$ according to (8). The top- and bottom-most points of the inclusion are embedded in the middle of high viscosity layers.

The overall patterns of shear rate distribution and structure evolution are retained as compared to the anisotropic host case. The shear rate in the low viscosity layers is approximately twice higher than in the $N_l = \infty$ case and virtually vanishes in the high viscosity layers. Isoclinal folds form mimicing the kink bands observed in the $N_l = \infty$ model. These fold stacks are pulled apart in the subsequent shearing stages and less inclined segments escape the tight folding stage. Similarly to the anisotropic case, no active propagation of the deformation bands is visible and even unfolding can be observed. The presence of strong layers causes the localized deformation to become less pronounced leading to smaller deflections within the folded bands.

We present structures for the cases $\delta = 2$, 10 and 100 at $\Gamma = 5$ in Fig. 4. The viscosity ratio is set at $m \approx 6$ and 400 for $\delta = 2$ and 100, respectively. In the $\delta = 2$ case, the structure can be described as a band of tightly folded markers that is inclined at 20° to the shear plane. The band is deflected towards the inclusion rim due to its rotation. The analytical model provides a good approximation to the structural evolution and the effect due to changing the layer thickness is small.

In the $\delta = 10$ case, the inclusion rotation is markedly reduced. The structure is more angular and a second, less prominent band of folds is present. Maximum fold amplitude is reduced but the flow perturbation extends deeper into the matrix. The orientation of the main deformation band is a little steeper than in the previous case. Increasing the layer thickness does not significantly change the inclusion rotation. For the finest layering, the structure is closely similar to that in the anisotropic matrix case and includes the secondary band of localized deformation. However, thick layering reduces the distance over which the inclusion perturbs the far-field flow. In addition, thicker layers prevent the formation of the isoclinal folds and secondary fold bands.

At $\delta = 100$, the inclusion rotation is strongly reduced relative to the rotation in the isotropic case. Fold amplitudes are markedly reduced and the deformation band is less prominent than in the previous cases. For $N_l = \infty$, marker deflections become ubiquitous in a sector between about 40° and 80° to the shear plane. The behavior is not observed for the finest discrete layering ($N_l = 33$) that is studied. The structure developed is strongly suppressed in the $N_l = 9$ case.

Evidently, the analytical anisotropic solution cannot be used to study the structural development for strong anisotropy and large deformation. The analytically modeled structures are only marginally dependent on the anisotropy factor and can be closely approximated by that for an isotropic matrix.

The analysis of Fig. 4 indicates that the rotation of the inclusion differs between different simulations and predominantly depends

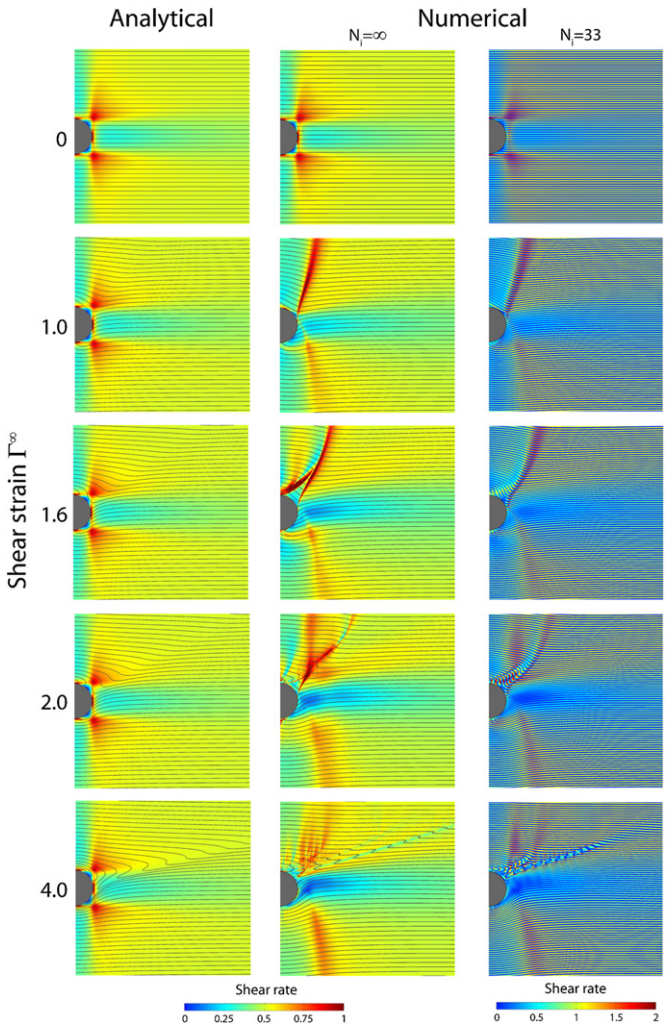


**Fig. 3.** Structure and shear rate distribution at $\Gamma^{\infty} = 0, 1, 1.6, 2, 4$. The results are shown for the anisotropic and layered host case with $N_I = 33$. The anisotropy factor equals 10 and the viscosity ratio is set accordingly. In the case of the anisotropic host and analytical model an arbitrarily spaced set of lines is used as passive markers. Note the difference in the colorbars. Two quadrants are required to show the results due to symmetry breaking. Only a small portion of the computational box is shown.

on $\delta$. The expected rotation of a rigid circular inclusion embedded in an isotropic matrix at $\Gamma = 5$ is 145°. The rates of the inclusion rotation as a function of the shear strain are shown in Fig. 5 for different $\delta$ and $N_I$.

The initial rotation rate deviates from the theoretical value of 0.5, which is equal to the background vorticity, and the deviation increases with increasing the anisotropy factor. In the $N_I \rightarrow \infty$ case, the effect is solely due to the proximity of boundaries and with decreasing the radius of the inclusion it disappears. Increasing the layer thickness leads to an additional decrease of the rotation rate. Here, we used the strong embedding, i.e. top and bottom of the inclusion are within strong layers. The effect is more prominent if the inclusion is embedded in weak layers.

The rotation rate curves show an overall decrease with strain. For $\delta = 2$, the rotation rate decreases to around 60% of the initial value. For $\delta = 10$, the rotation rate abruptly decreases at $\Gamma^{\infty} = 1.5$ and by $\Gamma^{\infty} = 2$ the inclusion effectively stagnates. For $\delta = 100$, even an antithetic rotation develops at $\Gamma^{\infty} = 3$ for $N_I = 33$. The net rotation of the inclusions is 100°, 50° and 20° at $\Gamma^{\infty} = 5$ for $\delta = 2$,10,100, respectively. The effect of the layer thickness on the rotation rate is irregular and rather small.

## 3. Discussion

### 3.1. Inclusion rotation

The rotation rate of a rigid circular inclusion embedded in an orthotropic infinite medium is zero in a pure shear flow. The behavior can be explained by line symmetry with respect to the shortening direction both for shortening parallel/normal to the anisotropy trace and in direction bisecting the previous two. For an arbitrarily oriented shortening direction, the solution is a superposition of the two solutions leaving the inclusion rotationless. Thus, the rotation rate is determined by the magnitude of the ambient vorticity, which equals half the shear rate in the case of simple shear.

The rotation rate that was numerically measured for the initial state of a planar anisotropy deviates from the theoretical value predicted for an infinite host. The deviation can be attributed to the proximity of dissimilar horizontal and vertical model boundaries. The boundary effect was recognized as a factor that can contribute to the stabilization of inclusions embedded in an isotropic host and occurring in spatially confined shear zones (Marques et al., 2005). For fixed spatial dimensions of the model, increasing the anisotropy factor leads to an increased perturbation range and a stronger boundary effect, see initial rotation rates in Fig. 5. Here, we do not present a detailed investigation of the boundary effect. Instead, we tried to keep it minimal in our simulations by using a sufficiently small inclusion radius with respect to the box height and width.

The initial rotation rate additionally decreases with increasing the thickness of layers. The reduction equals 20% of the limiting rate at the coarsest level studied and for the highest anisotropy factor. The deviation can be explained by the loss of orthotropic symmetry due to the presence of discrete layers.

The rotation rate decreases with strain already for $\delta = 2$ and shows a marked evolution for larger anisotropy factors. The structure that evolves around the inclusion is characterized by point symmetry only and the change of rotation rate is not unexpected. As some concerns may arise as to whether the rotation rate curves in Fig. 5 are affected by the boundary effect due to an increasing outreach of the structure with strain, we performed additional FEM simulations with an even smaller inclusion radius. The rotation rate curves remain largely unaffected showing that the structural development plays a predominant role on the inclusion rotation for the inclusion size of $R/H = 0.05$.

We found that changing the thickness of layers has an effect on both the inclusion rotation rate and the structural development. While the differences between the rotation rate curves are rather small even at late stages, the structures that develop around the inclusion differ appreciably. Looking at it from a different perspective, the presence of prominent fold trains reaching far into the host is not a prerequisite for a reduced rotation rate.

We propose the structural development as a new stabilization mechanism for a rigid circular inclusion embedded in a layered host subject to simple shear. The model, which is entirely based on continuum mechanics, provides an explanation to limited rotation of porphyroblasts by invoking the anisotropy of a layered host that is heterogeneously reoriented in progressing deformation. The mechanism is corroborated by the detection of snowball garnets recording a slow down of rotation rate with deformation as evidenced by Biermeier and Stuwe (2003). In our opinion, the slowing down rotation rate in this case is not necessarily related to a change in the ambient shear rate, as advocated by the authors, but could reflect an inherent behavior of rigid equidimensional inclusions as layered material is deflected in their surroundings.

The values of the anisotropy factor that we used in our study require some consideration. At equal fractions of low and high

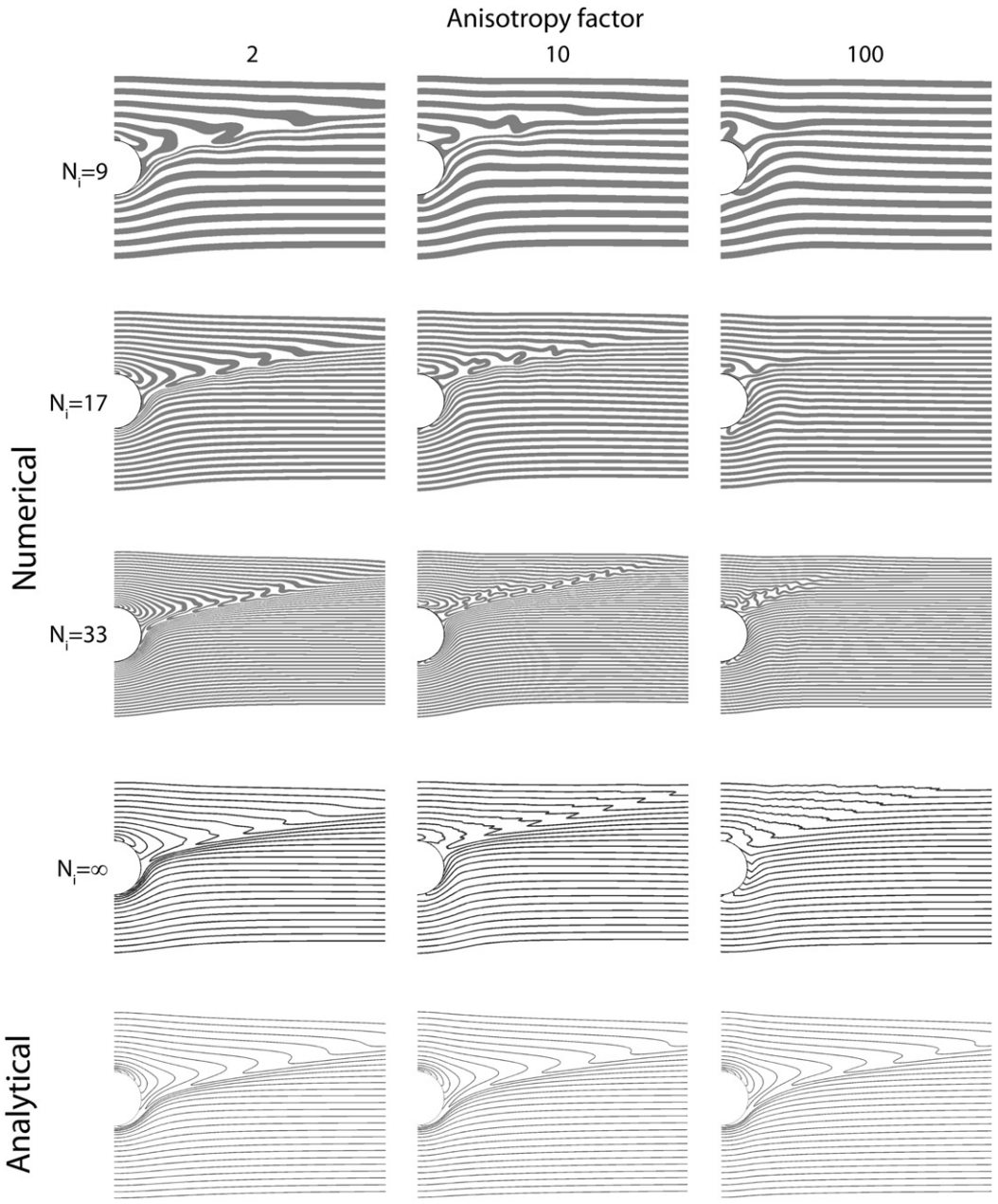


**Fig. 4.** Matrix structure at $\Gamma = 5$. Small portion of the computational domains displayed. Anisotropic factor $\delta$ is constant in columns, and the number of intersecting layers $N_l$ is fixed in rows. Structures obtained using the analytical solution are shown in the last row.

viscosity layers, the anisotropy factors $\delta = 2, 10$ and 100 correspond to viscosity ratios of ~6, 38 and 380, respectively. In our opinion, the intermediate case of $\delta = 10$ is arguably plausible to occur in natural shear zones. In this respect, an intrinsic anisotropy of layers may play an important role as it adds to the overall anisotropy. For example, Bayly (1970) estimated the anisotropy factor of mica-rich layers to exceed 12.5 based on measurements of characteristics of chevron fold developed in mica-poor and mica-rich sequences.

Using an initially unperturbed planar lamination around the inclusion appears to be merely a simplification in the model formulation. A modified model could be envisaged whereby an initially heterogeneous but isotropic host is gradually transformed into a layered medium or an early-stage foliation oriented at an angle to the shear direction is used at the onset of simulations. The effect of such transient stage on the inclusion rotation remains unknown. However, rigid inclusions such as garnets often grow syntectonically in an already layered host. Relaxing the constant radius assumption is probably the most needed modification of the presented model. Here, we can only speculate that the stabilization effect can be somewhat diminished at high growth to shear rates as the perturbed zone is progressively enclosed by the growing rigid rim. The model would also allow us to study the geometry of enclosed layers that could be directly compared to natural observations.

### 3.2. Structure development

The results of our large strain FEM simulations that allow for the non-planar, non-uniform lamination are strongly affected by the degree of host anisotropy. The effects related to anisotropy include

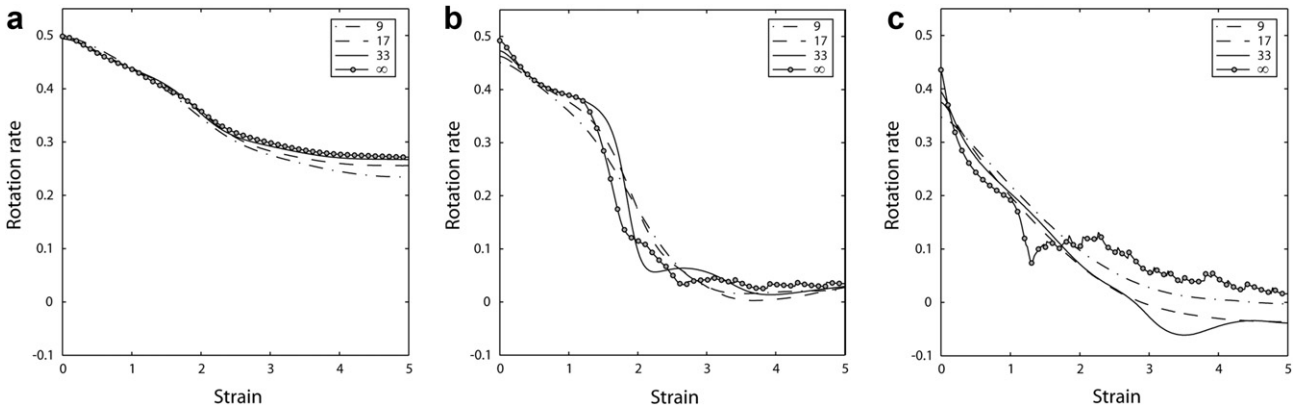


**Fig. 5.** Rotation rate of the inclusion for anisotropy factor $\delta = 2$ (a) 10 (b) and 100 (c) and $N_I = 9$, 17, 33 and $\infty$ as a function of shear strain $\Gamma^{\infty}$.

(1) a limited deflection of the markers adjacent to the inclusion stemming from a reduced rotation rate of the inclusion and (2) sharpening of the marker deflections in the major deformation band. The appearance of the subsidiary bands of localized shearing and the formation and propagation of related kink bands could be indicative of the host anisotropy. The kink bands undergo an initial active growth stage that is followed by band stiffening and transposition towards the shearing direction. The fact that the propagation is inhibited at late stages raises the general question of how far structural perturbations can propagate orthogonal to the shear plane in an anisotropic rock. The boundary effects should not be disregarded in this respect.

Increasing the anisotropy factor leads to a reduction of fold amplitudes on behalf of a pervasive development of internal instabilities. The latter requires high enough anisotropy factor and favorable orientation of the anisotropy trace. However, the structure in such regions is fundamentally irresolvable, as the length scale of the variations of the anisotropy direction is not dictated by the inclusion size in these regions. Hence, the structure becomes effectively scale-free, its evolution becomes mesh-size dependent and cannot be properly resolved despite the aggressive mesh adaptation that was employed in our simulations. The difficulty is also reflected in the rotation rate curves, where occasional sharp changes occur during remeshing stages (see Appendix).

A characteristic length scale may be introduced into the anisotropic model by incorporating the bending stiffness. Such a scheme, relying on a couple stress (micro-polar) formulation, has been proposed (e.g., Muhlhaus et al., 2002). Besides the obvious rationale that a finite length scale of the layering exists for real systems, employing such a code allows for circumventing the mesh sensitivity problem. Nevertheless, employing such a model will only partly solve the problem of approximating a layered material. Firstly, the upscaled model may fail if high spatial gradients of the layer thickness occur as it changes during the deformation. Furthermore, the rotation rate of the inclusion depends on how exactly the inclusion is embedded in the layered material, i.e. top and bottom in strong or weak layers. In this respect, the discrete layer approach is advantageous as it is free of any built-in uncertainties inherent to all upscaling techniques and yields relevant results to cases where relatively coarse layering/banding is present. The disadvantage is, however, the need for large numerical resolution. Nevertheless, some parameters such as the rotation rate as a function of strain are largely independent of the exact structure development in the matrix and may readily be studied with an upscaling approach. One may envision a hybrid model where the focus of interest is resolved explicitly and the more distal parts are treated with an effective material model.

Increasing the thickness of discrete layers remarkably reduces the perturbation range and largely affects the structure. The effect can be attributed to the bending stiffness of strong layers. The bending stiffness seems to prevent an active buckling from happening in the $\delta = 100$ and $N_I = 33$ case, while a pervasive internal instability is manifested in the complementary anisotropic model. In the coarsest model, the perturbation range is reduced to a degree that only a few open folds are formed. Folds like the one present in Fig. 4 for $\delta = 10$ and $N_I = 9$ are likely to be transported intact away from the inclusion along weak layers avoiding either isoclinal development or unfolding. These folds may appear rootless at even later stages.

Marques and Cobbold (1995) studied the formation of sheath folds around rigid inclusions embedded in a viscous host with passive layers subjected to simple shear flow in the far field. Marques et al. (2008) show how increasing the viscosity ratio between layers inhibits the development of strongly tubular folds. Despite the fact that the formation of sheath folds cannot be directly studied in our two-dimensional model, the tight and isoclinal folds that appear in our simulations could be considered as their preconditioners. In our model, the development of isoclinal folds is conditioned by the combined effect of the viscosity ratio and the ratio between the layer thickness and inclusion radius rather than the viscosity ratio alone.

The presented analytical solution was employed to approximate the flow in the non-planar, non-uniform case. However, the structures shown in Fig. 4 are only marginally dependent on the anisotropy factor for high strains and are very different than the structures modeled numerically. The solution should be used with caution if large rotations of the director field occur in the matrix causing a departure from the initial planar state of the host anisotropy.

## 4. Conclusions

A rigid circular inclusion embedded in an anisotropic host and subject to far-field simple shear is studied. An analytical solution is given for the initial state of planar anisotropy and the effects of large deformation and finite layering thickness are studied numerically using finite element models.

1) The matrix anisotropy has a prominent effect on the rotation rate of a rigid inclusion subject to simple shear in the far field. For the anisotropy factor $\delta = 10$, the net rotation of the inclusion yields 50° after shear strain $\Gamma = 5$, while the rotation of 145° is expected in the isotropic case. We propose the flow-induced perturbation of the host anisotropy around the inclusion as a stabilization mechanism in simple shear.

2) The structure developing around the inclusion is strongly affected by the host anisotropy. The layers intercepting the inclusion are markedly less deflected giving the impression of a smaller accumulated strain. Box folds and kink bands develop around the inclusion. The range of the flow perturbation increases with increasing anisotropy but the amplitude of folds is reduced.
3) The major effect of increasing the thickness of layers in the host is the reduction of the perturbation range. In the coarse limit, the formation of isoclinal recumbent folds is prevented and open folds result instead. These may in subsequent stages be advected away from the inclusion and appear as rootless structures.
4) In the limit of thin layering, the effective anisotropy provides a robust description of a layered medium. For high anisotropy factor, the inherent lack of a finite length scale in the anisotropic scheme leads to resolution problems and models with an inbuilt bending stiffness are preferred. Future numerical studies should address the problem of how robust such models are at the coarse layer thickness limit and with respect to non-uniform layer thickening.
5) Field studies that look at the behavior of heterogeneities in anisotropic materials should consider that the magnitude of inclusion rotation and foliation deflection around may yield appreciable strain underestimates when natural structures are interpreted without the effects of anisotropy taken into account.

## Acknowledgments

This work was supported by a Center of Excellence grant from the Norwegian Research Council to PGP. We would like to thank Ray Fletcher, Neil Mancketlow, Fernando Ornelas Marques and Dazhi Jiang for constructive comments regarding this work. We would also like to thank the Norwegian High Performance Computing (NOTUR) network to grant us machine access.

## Appendix. Numerical model

In this study, we have utilized our unstructured mesh FEM code MILAMIN implemented in MATLAB (Dabrowski et al., 2008). The use of an efficient self-developed implementation of FEM is necessitated by a large number of required timesteps and a high discretization level (>1,000,000 computational nodes).

A reliable mesh generator is required to create high quality unstructured meshes fitting interfaces between different layers and allowing for remeshing as complex structures evolve with deformation. For this purpose, we have chosen Triangle software developed by Shewchuk (2007). We find this software fast, robust and flexible. Furthermore, the possibility of an element area control existing in Triangle allows us to utilize better the power of an unstructured mesh approach employed in this study by refining the mesh in the vicinity of the inclusion and adapting it according to the local variations of the anisotropy direction.

Technical issues that have arisen during finite strain runs need some attention. By employing an unstructured mesh FEM, we have a possibility to update the mesh geometry according to the computed velocity field and continue with calculations. This Lagrangian approach has been used in both categories of the studied models. Advantageously, the advection of the material properties defined in integrations points such as anisotropy trace inclination is automatically taken care of. But a computational mesh must be occasionally regenerated to improve its quality that deteriorates after a number of updates. For the layered host case, we only need to track internal and external interfaces. However, inclinations of the anisotropy trace need to be interpolated to new integration points during this stage for the other category of our models. We have implemented an interpolation scheme in a spirit of krigging methods. The utilized scheme relies on identifying a prescribed amount of neighboring integration points (belonging to an old mesh), forming a radial basis functions and computing the corresponding weights in a way that enforces a collocation. Next, the radial basis functions are evaluated for the point of interest (i.e., new integration point) and together with the computed weights and inclinations defined in old integration points are used to compute a new value of the anisotropy orientation.

## References

Aerden, D., 2005. Comment on “Reference frame, angular momentum, and porphyroblast rotation” by Dazhi Jiang and Paul F. Williams. Journal of Structural Geology 27, 1128–1133.
Bayly, M.B., 1970. Viscosity and anisotropy estimates from measurements on chevron folds. Tectonophysics 9, 459.
Bell, T.H., Forde, A., Hayward, N., 1992a. Do smoothly curving, spiral-shaped inclusion trails signify porphyroblast rotation. Geology 20, 59–62.
Bell, T.H., Forde, A., Hayward, N., 1993. Do smoothly curving, spiral-shaped inclusion trails signify porphyroblast rotation – Reply. Geology 21, 480.
Bell, T.H., Johnson, S.E., 1989. Porphyroblast inclusion trails – The key to orogenesis. Journal of Metamorphic Geology 7, 279–310.
Bell, T.H., Johnson, S.E., Davis, B., Forde, A., Hayward, N., Wilkins, C., 1992b. Porphyroblast inclusion-trail orientation data – Eppure-non-son-girate. Journal of Metamorphic Geology 10, 295–307.
Biermeier, C., Stuwe, K., 2003. Strain rates from snowball garnet. Journal of Metamorphic Geology 21, 253–268.
Biot, M.A., 1965. Mechanics of Incremental Deformations: Theory of Elasticity and Viscoelasticity of Initially Stressed Solids and Fluids, Including Thermodynamic Foundations and Applications to Finite Strain. Wiley, New York.
Bjornerud, M.G., Zhang, H.B., 1994. Rotation of porphyroblasts in noncoaxial deformation - insights from computer-simulations. Journal of Metamorphic Geology 12, 135–139.
Bons, P.D., Jessell, M.W., Griera, A., Fay, C., Bell, T.H., Hobbs, B.E., 2009. Porphyroblast rotation versus nonrotation: conflict resolution! Geology 37, e182–e188.
Christensen, J.N., Rosenfeld, J.L., Depaolo, D.J., 1989. Rates of tectonometamorphic processes from rubidium and strontium isotopes in garnet. Science 244, 1465–1469.
Dabrowski, M., Krotkiewski, M., Schmid, D.W., 2008. MILAMIN: MATLAB-based finite element method solver for large problems. Geochemistry Geophysics Geosystems 9.
Fletcher, R.C., 2009. Deformable, rigid, and inviscid elliptical inclusions in a homogeneous incompressible anisotropic viscous fluid. Journal of Structural Geology 31, 382–387.
Gray, N.H., Busa, M.D., 1994. The 3-dimensional geometry of simulated porphyroblast inclusion trails – inert-marker, viscous-flow models. Journal of Metamorphic Geology 12, 575–587.
Hill, R., 1952. The elastic behaviour of a crystalline aggregate. Proceedings Physical Society of London A 65, 349–355.
Huddlestone-Holmes, C.R., Ketcham, R.A., 2010. An X-ray computed tomography study of inclusion trail orientations in multiple porphyroblasts from a single sample. Tectonophysics 480, 305–320.
Jiang, D.Z., 2001. Reading history of folding from porphyroblasts. Journal of Structural Geology 23, 1327–1335.
Jiang, D.Z., Williams, P.F., 2004. Reference frame, angular momentum, and porphyroblast rotation. Journal of Structural Geology 26, 2211–2224.
Johnson, S.E., 1993. Testing models for the development of spiral-shaped inclusion trails in garnet porphyroblasts – to rotate or not to rotate, that is the question. Journal of Metamorphic Geology 11, 635–659.
Johnson, S.E., 2009. Porphyroblast rotation and strain localization: debate settled! Geology 37, 663–666.
Lister, G.S., 1993. Do smoothly curving, spiral-shaped inclusion trails signify porphyroblast rotation – Comment. Geology 21, 479–480.
Mancktelow, N.S., Visser, P., 1993. The rotation of garnet porphyroblasts around a single fold, Lukmanier Pass, Central Alps – Reply. Journal of Structural Geology 15, 1369–1372.
Marques, F.G., Cobbold, P.R., 1995. Development of highly noncylindrical folds around rigid ellipsoidal inclusions in bulk simple shear regimes – Natural examples and experimental modeling. Journal of Structural Geology 17, 589.
Marques, F.O., Guerreiro, S.M., Fernandes, A.R., 2008. Sheath fold development with viscosity contrast: analogue experiments in bulk simple shear. Journal of Structural Geology 30, 1348–1353.
Marques, F.O., Taborda, R., Bose, S., Antunes, J., 2005. Effects of confinement on matrix flow around a rigid inclusion in viscous simple shear: insights from analogue and numerical modelling. Journal of Structural Geology 27, 379–396.

Muhlhaus, H.B., Dufour, F., Moresi, L., Hobbs, B., 2002. A director theory for visco-elastic folding instabilities in multilayered rock. International Journal of Solids and Structures 39, 3675–3691.
Passchier, C.W., Trouw, R.A.J., Zwart, H.J., Vissers, R.L.M., 1992. Porphyroblast rotation – Eppur-Si-Muove. Journal of Metamorphic Geology 10, 283–294.
Rosenfeld, J.L., 1970. Rotated garnets in metamorphic rocks.
Schmid, D.W., Podladchikov, Y.Y., 2003. Analytical solutions for deformable elliptical inclusions in general shear. Geophysical Journal International 155, 269–288.
Schmid, D.W., Podladchikov, Y.Y., 2004. Are isolated stable rigid clasts in shear zones equivalent to voids? Tectonophysics 384, 233–242.
Schoneveld, C., 1977. Study of some typical inclusion patterns in strongly paracrystalline-rotated Garnets. Tectonophysics 39, 453–471.
Shewchuk, J., 2007. Triangle, 1.6 ed..
Spry, A., 1963. The origin and significance of snowball structure in garnet. Journal of Petrology 4, 211.
ten Grotenhuis, S.M., Passchier, C.W., Bons, P.D., 2002. The influence of strain localisation on the rotation behaviour of rigid objects in experimental shear zones. Journal of Structural Geology 24, 485–499.
Williams, P.F., Jiang, D., 1999. Rotating garnets. Journal of Metamorphic Geology 17, 367–378.
Williams, P.F., Schoneveld, C., 1981. Garnet rotation and the development of axial-plane crenulation cleavage. Tectonophysics 78, 307–334.
Willis, J.R., 1964. Anisotropic elastic inclusion problems. Quarterly Journal of Mechanics and Applied Mathematics 17, 157.